E-proceedings of the 38th IAHR World Congress
September 1-6, 2019, Panama City, Panama
doi:10.3850/38WC092019-0576

LARGE EDDY SIMULATIONS OF FLOWS OVER A SUBMERGED WEIR

CHAEWOONG BAN [(1)] & SUNG-UK CHOI [(2)]

[(1)] *Department of Civil and Environmental Engineering, Yonsei University, Seoul, Republic of Korea*
blue8803@yonsei.ac.kr
[(2)] *Department of Civil and Environmental Engineering, Yonsei University, Seoul, Republic of Korea*
schoi@yonsei.ac.kr

ABSTRACT

Local scour downstream of a weir is a common problem that can result in serious damages to the weir itself. This study presents results from large eddy simulations (LESs) for surface jets over a submerged weir. Turbulent surface jets were computed over the flat and deformed beds due to scour for the same approach flow. The mean flow and turbulent statistics are presented for both flat and deformed bed conditions. Turbulent flows with the scour hole show that the reattachment region starting from the edge of the weir is located further downstream compared to the flows without scour. Furthermore, due to the presence of the scour hole, both average kinetic energy (AKE) and turbulent kinetic energy (TKE) increases and vertical gradient of the AKE become steeper compared to the flat bed case. This demonstrates that the capability of energy transfers from the AKE to the TKE increases by forming the scour hole on the flat bed.

Keywords: surface jet, large eddy simulation, mean flows, turbulent statistics, submerged weir

1 INTRODUCTION

The weir is a low-head instream structure constructed across the steam. The major role of the weir is to raise the upstream water level by blocking the flow. This decreases the velocity and facilitates sedimentation upstream of the weir. Albeit of its practical use, local scour downstream of the weir occurs and often threatens channel stability and safety of the weir itself. Therefore, identifying the generating mechanism of local scour downstream of the weir is of importance.

Local scour downstream of the weir can be attributed to the force exerted on the bed by highly 3D flows generated by the weir. Specifically, such flows are characterized by the massive separation and unsteady large-scale coherent structures. Laboratory or field experiments are, in general, difficult to obtain accurate information on the mean flow and turbulence statistics specially in the vicinity of the bed. Numerical studies using the conventional RANS approach do not provide information on the detailed turbulent structures which may play a key role in the scour process. This study attempted to present the mean flow and turbulent statistics of the surface over a submerged weir using the large eddy simulation (LES). The surface jets with and without the scour hole were simulated and LES results were used to investigate the generating mechanism of the scour hole.

2 GOVERNING EQUATIONS

Filtered Navier-Stokes equations governing the resolved quantities in LES were solved using OpenFOAM (Open Field Operation and Manipulation, Weller et al., 1998). The filtered Navier-Stokes equations are given by

$$\frac{\partial \bar{u}_i}{\partial x_i} \qquad [1]$$

$$\rho \frac{\partial \bar{u}_i}{\partial t} + \rho \bar{u}_j \frac{\partial \bar{u}_i}{\partial x_j} = -\frac{\partial \bar{p}}{\partial x_i} + \frac{\partial}{\partial x_j}\left(\bar{\tau}_{ij} + \tau_{ij}^{SGS}\right) \qquad [2]$$

which represents the conservation laws for mass and momentum, respectively. In. Eqs.[1] and [2], x_i is Cartesian coordinates (i = 1, 2, 3 corresponding to x, y, and z directions, respectively), t is the time, ρ is the fluid density, $\bar{u}_i$ is the instantaneous velocity vector, $\bar{u}_i$ is the filtered pressure, $\bar{\tau}_{ij}$ ($= \rho\nu\partial\bar{u}_i/\partial x_j$) is the filtered stress tensor associated with viscosity, and τ_{ij}^{SGS} ($= \rho\left(\bar{u}_i\bar{u}_j - \overline{u_i u_j}\right)$) is the subgrid-scale (SGS) stress tensor. The SGS stress tensor means the effect of the unresolved, small-scale turbulent motion, and this term is made up of isotropic and anisotropic components. Using the eddy-viscosity concept, the anisotropic part of the SGS stress tensor can be presented by

$$\tau_{ij}^{SGS} = \rho\left(\bar{u}_i\bar{u}_j - \overline{u_i u_j}\right) = 2\rho\nu_t\bar{S}_{ij} + \frac{1}{3}\delta_{ij}\tau_{kk}^{SGS} \qquad [3]$$

where ν_t is the kinematic eddy viscosity, δ_{ij} is the Kronecker delta, and $\bar{S}_{ij} = 1/2\left(\partial\bar{u}_i/\partial x_j + \partial\bar{u}_j/\partial x_i\right)$ is the filtered strain rate tensor.

In the present study, the wall-adapting local eddy viscosity (WALE) model, proposed by Nicoud and Ducros (1999), was imposed for the SGS model. The WALE model is capable of predicting correctly the asymptotic flow behavior of wall-bounded flows, since the SGS model uses information from the filtered velocity-gradient tensor $g_{ij}\left(=\partial\bar{u}_i/\partial x_j\right)$ to obtain the kinematic eddy viscosity (Weickert et al., 2010). For the WALE model, the kinematic eddy viscosity is calculated by

$$\nu_t = (C_w\overline{\Delta})^2 \frac{\left|\left(G_{ij}^a\right)\right|^{6/2}}{\left(\bar{S}_{ij}\bar{S}_{ij}\right)^{5/2}+\left|\left(G_{ij}^a\right)\right|^{5/2}} \qquad [4]$$

where C_w (= 0.325) is the WALE model constant, $\overline{\Delta}$ is the filter width, and G_{ij}^a is the traceless part of G_{ij} (= $1/2\left(g_{ik}g_{kj} + g_{jk}g_{ki}\right)$).

Eqs. [1] and [2] were solved using *pisoFoam* in OpenFOAM, which is an integrated solver for calculating the velocity-pressure correlation. In Eqs. [1] and [2], the temporal terms were discretized by a *backward* scheme. For the discretization of the convection term and diffusion term, *Gauss linearUpwind* scheme and *Gauss linear corrected* scheme were used, respectively. The second-order *Gauss linear* scheme was used for both the pressure-correction term and the pressure gradient term.

3 COMPUTATIONAL SETUP

The computational setup came from experimental conditions in Guan et al. (2014). Guan et al. performed laboratory experiments for local scour induced by flow over a submerged weir. The experimental flume was 12 m long and 0.44 m wide. The channel bed was covered with coarse sands with d_{50} = 0.85 mm. The topography of the scour hole and velocity were measured by 5 Hz multiple transducer arrays (MTAs) and an acoustic Doppler velocimeter with a sampling rate of 200 Hz, respectively. Table 1 lists the hydraulic conditions used in the Guan et al.'s experiments.

Table 1. Experimental conditions used by Guan et al. (2014).

Weir height, P (m)	Water depth, h (m)	Channel width, b (m)	Bulk velocity, u_b (m/s)	Shear velocity, u_* (m/s)	Reynolds number, Re	Froude number, Fr	Particle diameter, d_{50} (mm)
0.04	0.15	0.44	0.296	0.014	4.44 x 10^4	0.24	0.85

The computational domains for the flat bed (FB) and deformed bed (DB) cases are shown in Figures 1a and 1b, respectively. The length of the channel is 15 m, and the weir is located 10 m from the entrance. Figure 1c shows the enlarged snapshot for the grid configuration. Basically, the unstructured grid was used for the discretization and grid cells were refined near the impermeable boundary. If possible, regular hexahedrons were used for the base grid cells. To diminish the interpolation errors, grid non-orthogonality was minimized. The size of base grid cells was Δ = 5 x 10^{-3} m, which is $\Delta^+ = u_*\Delta/\nu$ = 70 in wall units. In the near wall region, the grid size is Δ = 0.625 x 10^{-3} m with a spatial average of $\Delta^+ \cong 3$ in wall units. The number of grid cells is about 2.7 x 10^7 and 2.6 x 10^7 for the FB case and the DB case, respectively. To obtain the developed flow, the LES was initially run for a time longer than $8t_e$. After the flow was fully developed, simulations were continued for a time longer than $25t_e$ to average flow statistics. The time step for the fine grid was 0.625 x 10^{-3} s. Detailed information about the computational grid and the simulation time are given in Table 2.

Table 2. Grid setup for LES computations.

Case	Total cell number (x 10^6)	Δ (x 10^{-3} m)		Δ^+ (near wall)	Δt (x 10^{-3} s)	Simulation time ($t_e = h/u_*$)	
		min	max			for developing	for averaging
FB	25.8	0.625	5	4	0.625	8	26
DB	27.2	0.625	5	4	0.625	9	25

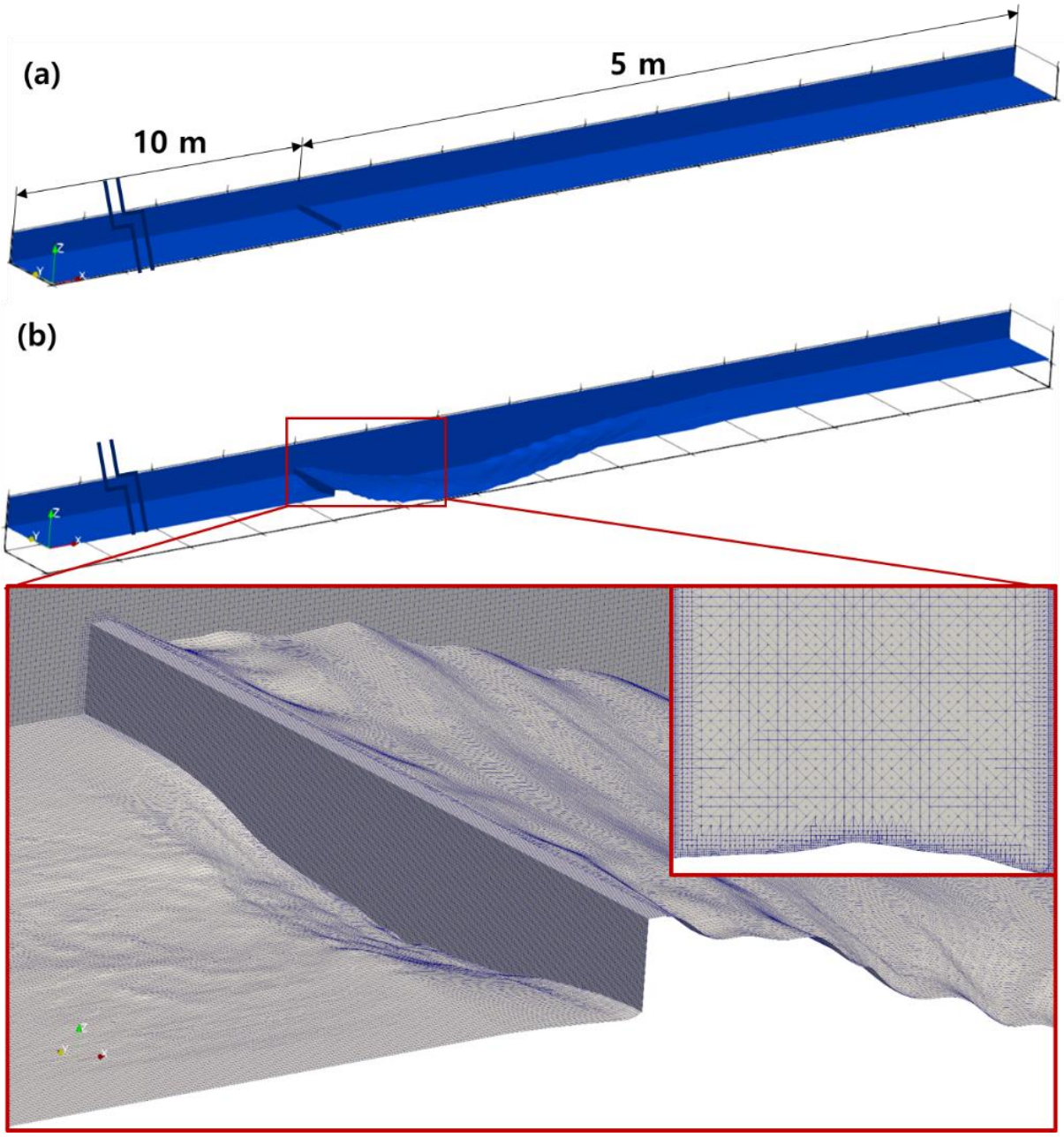

Figure 1. Computational domain and grids: (a) FB; (b) DB.

As for boundary conditions, a constant discharge was imposed at the inflow boundary. At walls including the sidewall, bed, and weir, the no-slip boundary condition was used. For the free surface boundary, the rigid-lid approximation was used. The use of the rigid-lid approximation can be justified for flows whose Froude number is less than 0.4 (Blanckaert & De Vriend, 2004). For the flow over the DB computed by the present LES, the Froude number based on the approach flow was 0.24, with the maximum Froude number about 0.4 in the vicinity of the weir.

4 RESULTS AND DISCUSSIONS

4.1 Mean flows

Vertical distributions of the time-averaged streamwise velocity ($\langle\bar{u}\rangle$) at 10 verticals for the DB case computed by LES are shown in Figure 2. The LES results were plotted together with measured data by Guan et al. (2014). It appears that the simulated results compare favorably to the measured data. In particular, the velocity distribution exhibits well the development of the boundary layer after passing the weir. Specifically, the flow accelerates by passing over the weir and forms the separated shear layer resulting from the weir. In addition, the velocity profiles in the scour hole indicate that vortex-dominated flows are formed by the separated shear layer.

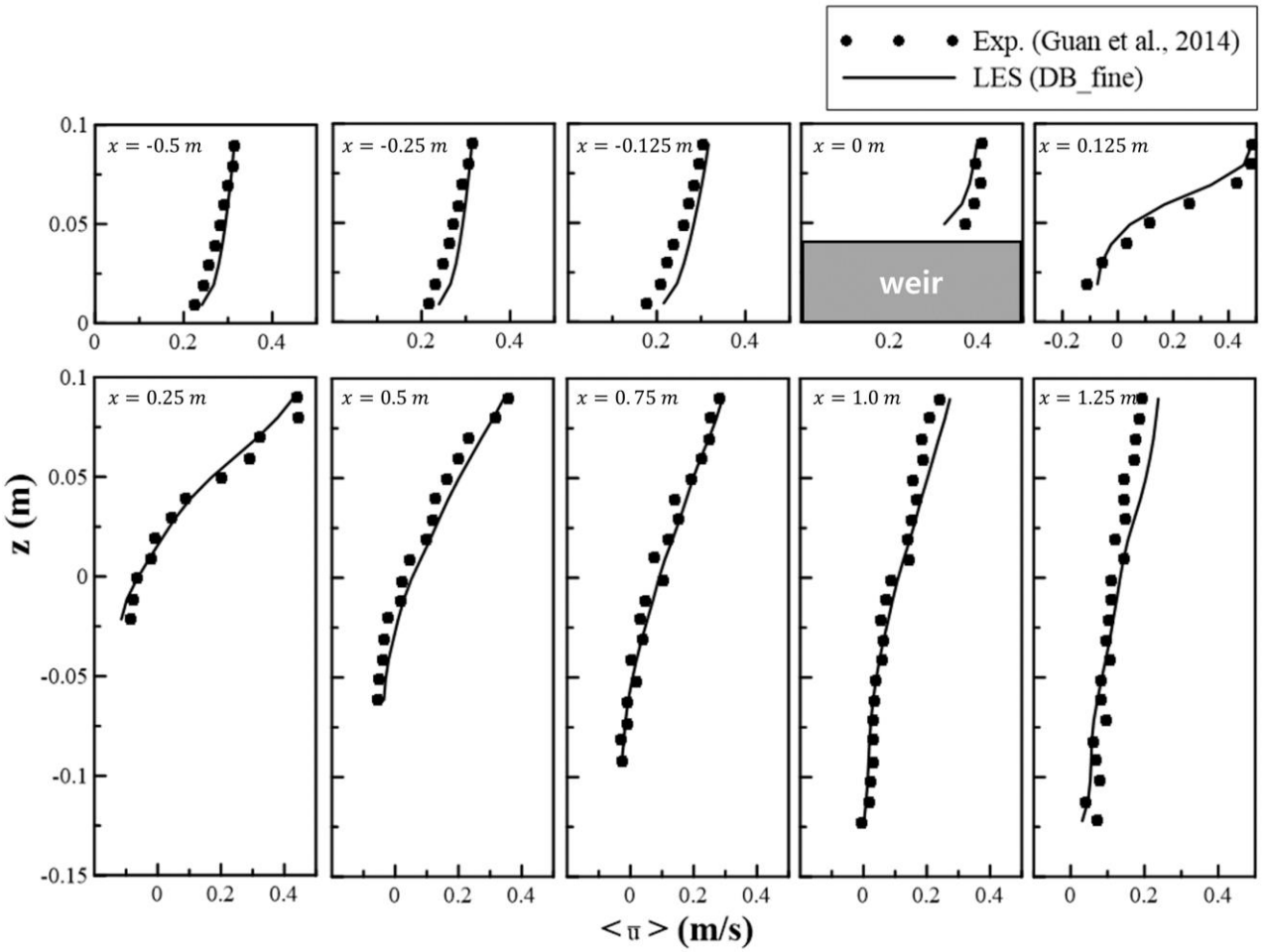

Figure 2. Time-averaged streamwise velocity over the DB along the centerline ($y/b = 0.5$).

Figures 3a and 3b show contour plots of the time-averaged streamwise velocity ($\langle\overline{u}\rangle$), with streamlines for the FB and DB cases, respectively. It can be seen that the flow contracts due to the weir and expands vertically after passing the weir. The separated shear layer, starting to develop at the tip of the weir, is observed near the bottom for both FB and DB cases. However, the separated shear layer for the DB case is much longer than that for the FB case. In the figures, the height at which $\langle\overline{u}\rangle$ = 0 was connected by a red line after the weir to identify the separated shear layer. That is, the separated shear layer starts to develop at the tip of the weir (x = 0) and ends at the reattachment point ($x = x_r$). The length of the red line is about the extent of the recirculation region, and the backward flows occur below this red line. In the FB case, the weak vortex is observed immediately downstream of the weir. Successively, a large vortex, the length of which is about 0.30 m in the major axis, appears, rotating in the direction opposite to the weak vortex. In the FB case, the reattachment point is found to be x_r = 0.34 m. The backward flows extend from the reattachment point to a location right before the weak vortex. In the DB case, the vortical structure changes significantly. That is, the primary vortex is extended along the bottom slope of the scour hole, with the weak vortex disappeared. Compared with the FB case, the reattachment point is observed to move further downstream, i.e., x_r = 1.05 m. In Guan et al.'s (2014) experiments, the maximum scour occurred at x = 1.06 m, which is sufficiently close to the reattachment point computed by LES.

Contour plots of the time-averaged vertical velocity ($\langle\overline{w}\rangle$) are given with streamlines in Figures 4a and 4b for the FB and DB cases, respectively. In both figures, the range and the intensity of the downflows are clearly seen. That is, the downflows in the FB case appear to be much stronger than those in the DB case, and these strong downflows are thought to be the major source of generating the scour hole. In the wall region (z/h < 0.2) of the FB case, the maximum downflows of $\langle\overline{w}\rangle$ = -0.021 m/s occur at x = 0.30 m, which is very close to the reattachment point. For 0.22 < x < 0.42 m, the downflows are found to be strong, so that the absolute value of $\langle\overline{w}\rangle$ is larger than 0.020 m/s. In the wall region of the DB case, the maximum downflows of $\langle\overline{w}\rangle$ = -0.007 m/s occur at x = 0.60 m. The location of the maximum downflows is very close to the downstream end of the primary vortex, which is significantly different from the reattachment point. In the DB case, the downflows do not appear to be strong over the entire scour hole, with an absolute value of $\langle\overline{w}\rangle$ less than 0.007 m/s.

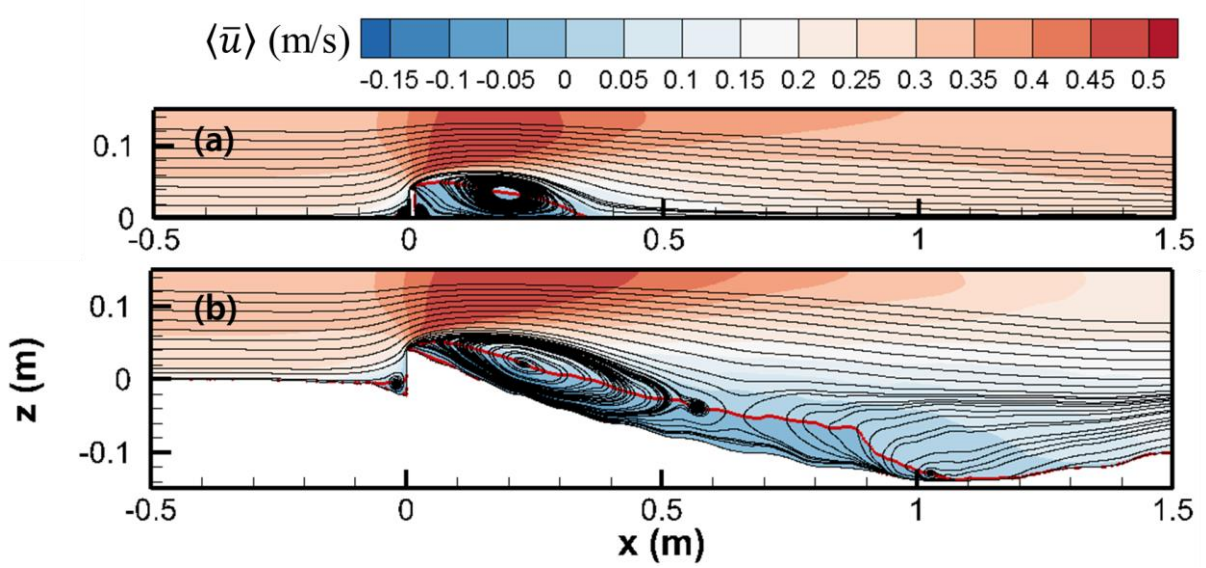

Figure 3. Contours of time-averaged streamwise velocity with streamlines: (a) FB; (b) DB.

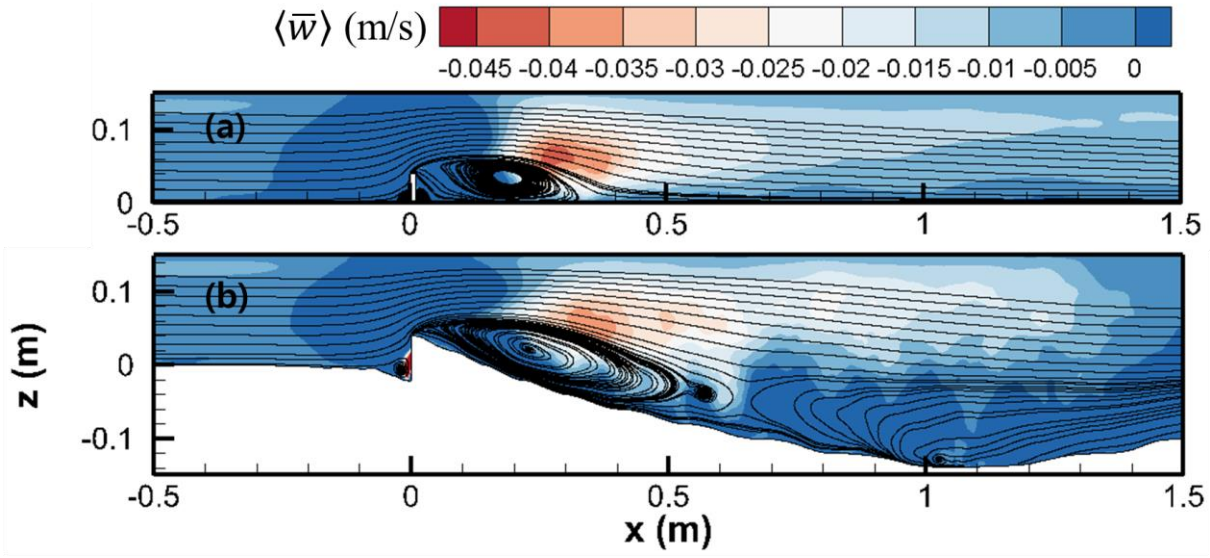

Figure 4. Contours of time-averaged vertical velocity with streamlines: (a) FB; (b) DB.

4.2 Turbulence statistics

For the surface jet over the weir, the change in the turbulence statistics with the development of the scour hole is examined. Here, the turbulence statistics include AKE and TKE, which are calculated, respectively, by

$$AKE = \frac{\langle\bar{u}\rangle^2+\langle\bar{v}\rangle^2+\langle\bar{w}\rangle^2}{u_b^2} \qquad [5a]$$

$$TKE = \frac{\langle\bar{u}'^2\rangle+\langle\bar{v}'^2\rangle+\langle\bar{w}'^2\rangle}{u_b^2} \qquad [5b]$$

where AKE and TKE are normalized by the bulk velocity (u_b). In Eqs. [5a] and [5b], AKE and TKE denotes the energies from the mean flow and from turbulent fluctuations, respectively.

Figures 5a and 5b present distributions of the AKE by LES for the FB and DB cases, respectively. It can be seen that, after passing the tip of the weir, the AKE increases rapidly, showing the maximum, and decreases gradually in the downstream direction. This is of course due to flow contraction by the weir. For the DB case, near the bed immediately downstream of the weir, a local maximum AKE of 0.1 is seen in the recirculation region, which is obviously due to the recirculation vortex. For the DB case, the vertical gradient of the AKE is steep up to x = 1.0 m, which can be compared with the FB case, where the vertical gradient is steep up to x = 0.3 m. The steeper the vertical gradient of the AKE, the more the turbulent momentum flux exchanges in the vertical direction. Therefore, in the DB case, the mean flow dissipates more kinetic energy due to the presence

of the scour hole where the momentum transfer takes place more actively by extending the length of the separated shear layer. This indicates that more AKE is transferred to TKE because of the scour hole for the DB case compared with the FB case.

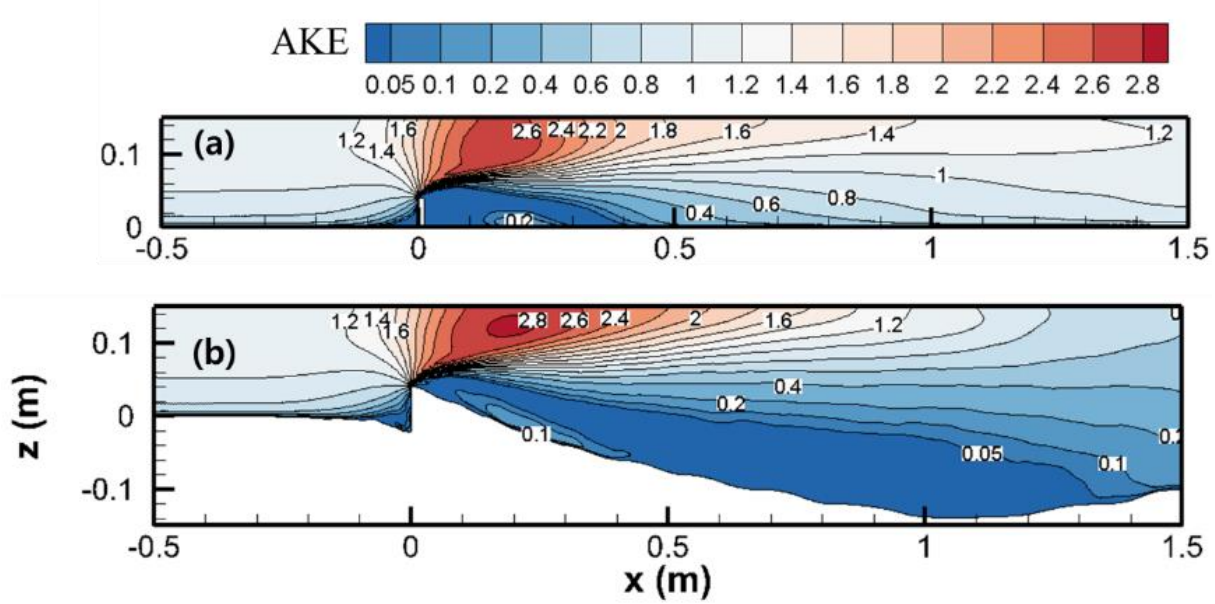

Figure 5. Distributions of AKE: (a) FB; (b) DB.

Figures 6a and 6b present TKE distributions by LES for the FB and DB cases, respectively. The TKE distribution for the DB case measured by Guan et al. (2014) is also given in Figure 6c. Clearly, the TKE distribution for the DB case by LES compares well with that by Guan et al. (2014). A general feature of the TKE distribution for the DB case observed in the figure is that the TKE is relatively high along the downslope of the scour hole and it decreases gradually along the upslope. A similar trend in the TKE distribution was also observed in laboratory experiments for the surface jet (Ben Meftah and Mossa, 2006) and for the impinging jet (Si et al., 2018). The TKE difference between the downslope and the upslope is the result of a high rate of TKE dissipation in the scour hole.

The maximum TKE for the DB case is 0.28, whereas the maximum TKE for the FB case is 0.2. Both maximum TKEs occur at the same streamwise distance, x = 0.28 m. However, the maximum TKE for the FB case occurs 0.05 m above the bed, while that for the DB case occurs 0.08 m above the bed. This indicates more intensive turbulence fluctuations close to the bed in the FB case. In the wall region (z/h < 0.2), the TKE is larger than 0.12 for 0.28 < x < 0.38 m in the FB case, while it is larger than 0.06 for 0.2 < x < 0.5 m in the DB case. That is, the TKE in the wall region is larger downstream of the weir without the scour hole, and this larger TKE may be the major source of creating the scour hole downstream.

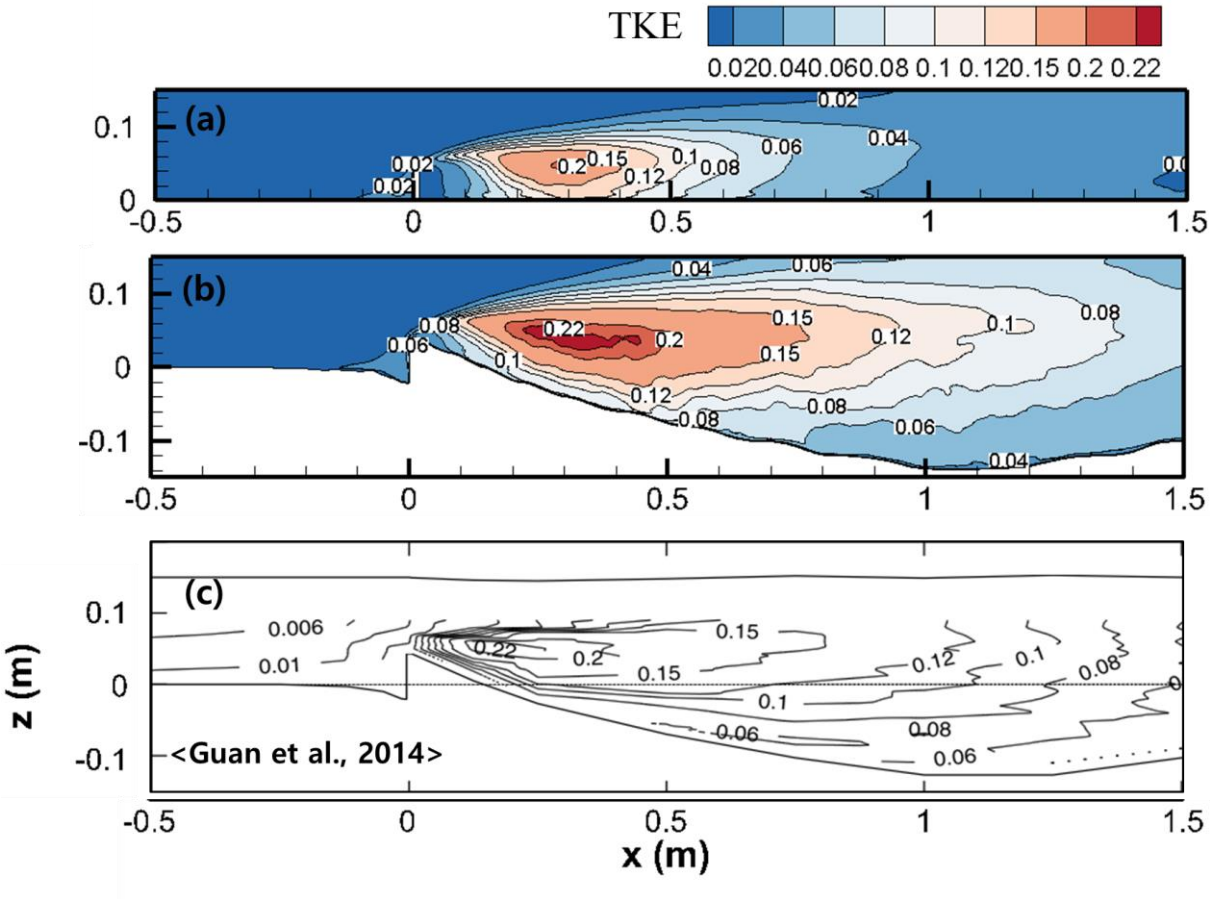

Figure 6. Distributions of TKE: (a) FB (LES); (b) DB (LES); (c) DB (exp.).

5 CONCLUSIONS

Highly resolved LES was carried out for turbulent surface jets over a submerged weir under FB and DB conditions. The LES results provided thorough statistical descriptions of such flows, and comparisons with available experimental data showed good agreement.

The presence of the weir and developed scour hole affect not only the mean flow but also turbulent structures downstream of the submerged weir. For both FB and DB cases, maximum downflows occur at the downstream end of the primary vortex, regardless of the presence of a scour hole. In the DB case, the primary vortex in the separated shear layer is extended longitudinally, locating the reattachment point further downstream, and the downflows are weakened. The maximum AKE for the DB case is larger than that for the FB case, but the AKE is significantly weakened near the bed in the DB case. This indicates that the capability of energy transfer from AKE to TKE increases in the presence of the scour hole. This conforms to the TKE distribution for the DB case, where the overall TKE increases.

In summary, the LES results indicated that major contribution to creating the scour hole downstream of the weir is provided by the strengthened downflows and TKE distribution of the surface jet.

ACKNOWLEDGEMENTS

This research was supported by a grant (18CTAP-C132929-02) from Infrastructure and transportation technology promotion research Program funded by Ministry of Land, Infrastructure and Transport of Korean government.

REFERENCES

Ben Meftah, M., & Mossa, M. (2006). Scour holes downstream of bed sills in low-gradient channels. *Journal of Hydraulic Research*, 44(4), 497-509.

Blanckaert, K., & De Vriend, H.J. (2004). Secondary flow in sharp open-channel bends. *Journal of Fluid Mechanics*, 498, 353-380.

Guan, D., Melville, B.W., & Friedrich, H. (2014). Flow patterns and turbulence structures in a scour hole downstream of a submerged weir. *Journal of Hydraulic Engineering*, 140(1), 68-76.

Nicoud, F., & Ducros, F. (1999). Subgrid-scale stress modelling based on the square of the velocity gradient tensor. *Flow, Turbulence and Combustion*, 62(3), 183-200.

Rajaratnam, N., & Muralidhar, D. (1969). Flow below deeply submerged rectangular weirs. *Journal of Hydraulic Research*, 7(3), 355-374.

Si, J.H., Lim, S.Y., & Wang, X.K. (2018). Flow structures in evolving scour holes caused by a plunging jet downstream of a weir. *Journal of Hydraulic Engineering*, 144(6), 04018018.

Weickert, M., Teike, G., Schmidt, O., & Sommerfeld, M. (2010). Investigation of the LES WALE turbulence model within the lattice Boltzmann framework. *Computers & Mathematics with Applications*, 59(7), 2200-2214.

Weller, H.G., Tabor, G., Jasak, H., & Fureby, C. (1998). A tensorial approach to computational continuum mechanics using object-oriented techniques. *Computers in Physics*, 12(6), 620-631.

